# Electron-lattice and strain effects in manganite heterostructures: The case of a single interface

A. Iorio, C. A. Perroni, V. Marigliano Ramaglia, and V. Cataudella
*CNR-SPIN and Dipartimento di Scienze Fisiche, Università degli Studi di Napoli Federico II, Complesso Universitario Monte S. Angelo, Via Cintia, I-80126 Napoli, Italy*

(Received 16 September 2010; revised manuscript received 6 January 2011; published 23 February 2011)

A correlated inhomogeneous mean-field approach is proposed to study a tight-binding model of the manganite heterostructures $(LaMnO_3)_{2n}/(SrMnO_3)_n$ with average hole doping $x = 1/3$. Phase diagrams and spectral and optical properties of large heterostructures (up to 48 sites along the growth direction) with a single interface are discussed, and the effects of electron-lattice antiadiabatic fluctuations and strain are analyzed. The formation of a metallic ferromagnetic interface is quite robust upon varying the strength of electron-lattice coupling and strain, though the size of the interface region is strongly dependent on these interactions. The density of states never vanishes at the chemical potential due to the formation of the interface, but it shows a rapid suppression with increasing the electron-lattice coupling. The in-plane and out-of-plane optical conductivities show sharp differences since the in-plane response has metallic features, while the out-of-plane one is characterized by a transfer of spectral weight to high frequency. The in-plane response mainly comes from the region between the two insulating blocks, so that it provides a clear signature of the formation of the metallic ferromagnetic interface. Results are discussed in connection with available experimental data.

DOI: 10.1103/PhysRevB.83.085107 PACS number(s): 73.20.−r, 73.40.−c, 73.50.−h

## I. INTRODUCTION

Transition-metal oxides are of great current interest because of the wide variety of the ordered phases that they exhibit and the strong sensitivity to external perturbations.[1] Among them, manganese oxides with the formula $R_{1-x}A_xMnO_3$ ($R$ stands for a rare earth such as La, $A$ represents a divalent alkali element such as Sr or Ca, and $x$ is the hole doping), known as manganites, have been studied intensively both for their very rich phase diagram and for the phenomenon of colossal magnetoresistance.[2] This effect is often exhibited in the doping regime $0.2 < x < 0.5$, where the ground state of the systems is ferromagnetic. The ferromagnetic phase is usually explained by invoking the double-exchange mechanism in which hopping of an outer-shell electron from a $Mn^{3+}$ to a $Mn^{4+}$ site is favored by a parallel alignment of the core spins.[3] In addition to the double-exchange term that promotes hopping of the carriers, a strong interaction between electrons and lattice distortions plays a non-negligible role in these compounds, giving rise to the formation of polaron quasiparticles.[4]

Very recently, high-quality atomic-scale "digital" heterostructures consisting of a combination of transition-metal oxide materials have been realized. Indeed, heterostructures represent the first steps to use correlated oxide systems in realistic devices. Moreover, at the interface, the electronic properties can be drastically changed in comparison with those of the bulk. Recent examples include the formation of a thin metallic layer at the interface between band and Mott insulators, such as, for example, between $SrTiO_3$ (STO) and $LaTiO_3$ oxides[5] or between the band insulators[6] $LaAlO_3$ and STO.

Very interesting examples of heterostructure are given by the superlattices $(LaMnO_3)_m/(SrMnO_3)_n$ with $n/(m+n)$ average hole doping.[7] Here $LaMnO_3$ (LMO) (one electron per Mn $e_g$ state) and $SrMnO_3$ (SMO) (no electrons per Mn $e_g$ state) are the two end-member compounds of the alloy $La_{1-x}Sr_xMnO_3$ and are both antiferromagnetic insulating. In these systems, not only the chemical composition but also the thickness of the constituent blocks specified by $m$ and $n$ is important for influencing the properties of superlattices. Focus has been on the case $m = 2n$ corresponding to the average optimal hole doping $x = 1/3$.[8,9] The superlattices exhibit a metal-insulator transition as a function of temperature for $n \leqslant 2$ and behave as insulators for $n \geqslant 3$. The superlattices undergo a rich variety of transitions among metal, the Mott variable range hopping insulator, the interaction-induced Efros-Shklovskii insulator, and the polaronic insulator.[10]

Interfaces play a fundamental role in tuning the metal-insulator transitions since they control the effective doping of the different layers. Even when the system is globally insulating ($n \geqslant 3$), some nonlinear optical measurements suggest that, for a single interface, ferromagnetism due to the double-exchange mechanism can be induced between the two antiferromagnetic blocks.[11] Moreover, it has been found that the interface density of states exhibits a pronounced peak at the Fermi level whose intensity correlates with the conductivity and magnetization.[12] These measurements point toward the possibility of a two-dimensional half-metallic gas for the double layer[13] whose properties have been studied by using *ab initio* density-functional approaches.[14] However, up to now, this interesting two-dimensional gas has not been experimentally assessed in a direct way by using lateral contacts on the region between the LMO and SMO blocks.

In analogy with thin films, strain is another important quantity to tune the properties of manganite heterostructures. For example, far from interfaces, inside LMO, electron localization and local strain favor antiferromagnetism and $e_g$ $(3z^2 - r^2)$ orbital occupation.[15] The magnetic phase in LMO is compatible with the $C$ type.[2] Moreover, by changing the substrate, the ferromagnetism in the superlattice can be stabilized.[16]

From a theoretical point of view, in addition to *ab initio* calculations, tight-binding models have been used to study manganite superlattices. The effects of magnetic

 

and electron-lattice interactions on the electronic properties have been investigated going beyond adiabatic mean-field approximations.[17,18] However, the double layer with large blocks of LMO and SMO has not been studied much. Moreover, the effects of strain have been analyzed only within mean-field approaches.[19]

In this paper, we have studied phase diagrams and spectral and optical properties for a very large bilayer $(LMO)_{2n}/(SMO)_n$ (up to 48 planes relevant for a comparison with fabricated heterostructures) starting from a tight-binding model. We have developed a correlated inhomogeneous mean-field approach taking into account the effects of electron-lattice antiadiabatic fluctuations. Strain is simulated by modulating hopping and spin-spin interaction terms. We have found that a metallic ferromagnetic interface forms for a large range of the electron-lattice couplings and strain strengths. For this regime of parameters, the interactions are able to change the size of the interface region. We find the magnetic solutions that are stable at low temperature in the entire superlattice. The general structure of our solutions is characterized by three phases running along the growth $z$ direction: an antiferromagnetic phase with localized or delocalized (depending on the model parameters) charge carriers inside the LMO block, a ferromagnetic state at the interface with itinerant carriers, and a localized polaronic $G$-type antiferromagnetic phase inside the SMO block. The type of antiferromagnetic order inside LMO depends on the strain induced by the substrate.

We have discussed the spectral and optical properties corresponding to different parameter regimes. Due to the formation of the metallic interface, the density of states is finite at the chemical potential. With increasing the electron-phonon interaction, it gets reduced at the chemical potential, but it never vanishes even in the intermediate to strong electron-phonon coupling regime. Finally, we have studied both the in-plane and out-of-plane optical conductivities, pointing out that they are characterized by marked differences: the former shows a metallic behavior, the latter a transfer of spectral weight at high frequency due to the effects of the electrostatic potential well trapping electrons in the LMO block. The in-plane response at low frequency is mainly due to the region between the two insulating blocks, so that it can be used as a tool to assess the formation of the metallic ferromagnetic interface.

The paper is organized as follows: In Sec. II, the model and variational approach are introduced; in Sec. III, the results regarding static properties and phase diagrams are discussed; in Sec. IV, the spectral properties are analyzed; in Sec. V, the optical conductivities are analyzed; and conclusions are presented in the final section.

## II. THE VARIATIONAL APPROACH

### A. Model Hamiltonian

For manganite superlattices, the Hamiltonian of the bulk $H_0$ has to be supplemented by Coulomb terms representing the potential arising from the pattern of the La and Sr ions,[20] thus

$$H = H_0 + H_{\mathrm{Coul}}. \tag{1}$$

To set up an appropriate model for the double layer, it is important to take into account the effects of the strain. The epitaxial strain produces the tetragonal distortion of the $MnO_6$ octahedron, splitting the $e_g$ states into $x^2$-$y^2$ and $3z^2$-$r^2$ states.[19] If the strain is tensile, $x^2$-$y^2$ is lower in energy, while if the strain is compressive, $3z^2$-$r^2$ is favored. In the case of $n = 8$ with three interfaces,[15] the superlattices grown on STO are found to be coherently strained: all of them are forced to the in-plane lattice parameter of substrate and to an average out-of-plane parameter $c \simeq 3.87$ Å.[15] As a consequence, one can infer that LMO blocks are subjected to compressive strain ($-2.2\%$) and SMO blocks to tensile strain ($+2.6\%$). For the case of the LMO block, the resulting higher occupancy of $3z^2$-$r^2$ enhances the out-of-plane ferromagnetic interaction owing to the larger electron hopping out-of-plane. For the case of the SMO block, the reverse occurs. A suitable model for the bilayer has to describe the dynamics of the $e_g$ electrons, which in the LMO and SMO blocks preferentially occupy the more anisotropic $3z^2$-$r^2$ orbitals and more isotropic $x^2$-$y^2$ orbitals, respectively. For this reason, in this paper we adopt an effective single-orbital approximation for the bulk manganite.

The model for the bulk takes into account the double-exchange mechanism, the coupling to the lattice distortions, and the superexchange interaction between neighboring localized $t_{2g}$ electrons on Mn ions. The coupling to longitudinal optical phonons arises from the Jahn-Teller effect that splits the $e_g$ double degeneracy. Then, the Hamiltonian $H_0$ reads

$$\begin{aligned} H_0 = &- \sum_{\vec{R}_i,\vec{\delta}} t_{|\vec{\delta}|} \left( \frac{S_0^{\vec{R}_i,\vec{R}_i+\vec{\delta}} + 1/2}{2S+1} \right) c^\dagger_{\vec{R}_i} c_{\vec{R}_i+\vec{\delta}} \\ &+ \omega_0 \sum_{\vec{R}_i} a^\dagger_{\vec{R}_i} a_{\vec{R}_i} + g\omega_0 \sum_{\vec{R}_i} c^\dagger_{\vec{R}_i} c_{\vec{R}_i} \left( a_{\vec{R}_i} + a^\dagger_{\vec{R}_i} \right) \\ &+ \frac{1}{2} \sum_{\vec{R}_i,\vec{\delta}} \epsilon_{|\vec{\delta}|} \vec{S}_{\vec{R}_i} \cdot \vec{S}_{\vec{R}_i+\vec{\delta}} - \mu \sum_{\vec{R}_i} c^\dagger_{\vec{R}_i} c_{\vec{R}_i}. \end{aligned} \tag{2}$$

Here $t_{|\vec{\delta}|}$ is the transfer integral of electrons occupying $e_g$ orbitals between nearest-neighbor (NN) sites, $S_0^{\vec{R}_i,\vec{R}_i+\vec{\delta}}$ is the total spin of the subsystem consisting of two localized spins on NN sites and the conduction electron, $\vec{S}_{\vec{R}_i}$ is the spin of the $t_{2g}$ core states ($S = 3/2$), and $c^\dagger_{\vec{R}_i}(c_{\vec{R}_i})$ creates (destroys) an electron with spin parallel to the ionic spin at the $i$th site in the $e_g$ orbital. The coordination vector $\vec{\delta}$ connects NN sites. The first term of the Hamiltonian describes the double-exchange mechanism in the limit where the intra-atomic exchange integral $J$ is much larger than the transfer integral $t_{|\vec{\delta}|}$. Furthermore, in Eq. (2), $\omega_0$ denotes the frequency of the local optical-phonon mode, $a^\dagger_{\vec{R}_i}(a_{\vec{R}_i})$ is the creation (annihilation) phonon operator at the site $i$, and the dimensionless parameter $g$ indicates the strength of the electron-phonon interaction. Finally, in Eq. (2), $\epsilon_{|\vec{\delta}|}$ represents the antiferromagnetic superexchange coupling between two NN $t_{2g}$ spins and $\mu$ is the chemical potential. The hopping of electrons is supposed to take place between the equivalent NN sites of a simple cubic lattice (with finite size along the $z$ axis corresponding to the growth direction of the heterostructure) separated by the distance $|n - n'| = a$. The units are such that

the Planck constant $\hbar = 1$, the Boltzmann constant $k_B = 1$, and the lattice parameter $a = 1$.

Regarding the terms due to the interfaces, one considers that $La^{3+}$ and $Sr^{2+}$ ions act as $+1$ charges of magnitude $e$ and neutral points, respectively. In the heterostructure, the distribution of those cations induces an interaction term for $e_g$ electrons of Mn giving rise to the Hamiltonian

$$H_{\text{Coul}} = \sum_{\vec{R}_i \neq \vec{R}_j} \frac{1}{2\epsilon_d} \frac{e^2 n_{\vec{R}_i} n_{\vec{R}_j}}{|\vec{R}_i - \vec{R}_j|} + \sum_{\vec{R}_i^{\text{La}} \neq \vec{R}_j^{\text{La}}} \frac{1}{2\epsilon_d} \frac{e^2}{|\vec{R}_i^{\text{La}} - \vec{R}_j^{\text{La}}|} - \sum_{\vec{R}_i, \vec{R}_j^{\text{La}}} \frac{1}{\epsilon_d} \frac{e^2 n_{\vec{R}_i}}{|\vec{R}_i - \vec{R}_j^{\text{La}}|}, \tag{3}$$

with $n_{\vec{R}_i} = c^\dagger_{\vec{R}_i} c_{\vec{R}_i}$ the electron occupation number at the Mn site $i$, $\vec{R}_i$ and $\vec{R}_i^{\text{La}}$ are the positions of Mn and $La^{3+}$ in the $i$th unit cell, respectively, and $\epsilon_d$ is the dielectric constant of the material. In our calculation, the long-range Coulomb potential has been modulated by a factor $\eta$ inducing a fictitious finite screening length (see Appendix). This factor was added only for computational reasons since it allows us to calculate the summations of the Coulomb terms over the lattice indices. We have modeled the heterostructures as slabs whose in-plane size is infinite.

To describe the magnitude of the Coulomb interaction, we define the dimensionless parameter $\alpha = e^2/(a\epsilon_d t_{|\vec{\delta}|})$, which controls the charge-density distribution. The order of magnitude of $\alpha$ can be estimated from the hopping parameter $t_{|\vec{\delta}|} \sim 0.65$ eV, lattice constant $a = 4$ Å, and typical value of the dielectric constant $\epsilon \sim 10$ to be around 0.2.

Strain plays an important role also by renormalizing the heterostructure parameters. Strain effects can be simulated by introducing an anisotropy into the model between the in-plane hopping amplitude $t_{\delta_{||}} = t$ (with $\delta_{||}$ indicating nearest neighbors in the $x$-$y$ planes) and out-of-plane hopping amplitude $t_{|\delta_z|} = t_z$ (with $\delta_z$ indicating nearest neighbors along the $z$ axis).[21] Moreover, the strain induced by the substrate can directly affect the patterns of core spins.[22] Therefore, in our model, we have also considered the anisotropy between the in-plane superexchange energy $\epsilon_{|\delta_{||}|} = \epsilon$ and the out-of-plane one $\epsilon_{|\delta_z|} = \epsilon_z$. We have found that the stability of magnetic phases in LMO blocks is influenced by the presence of compressive strain, while in SMO the sensitivity to strain is poor. Therefore, throughout the paper, we take as reference the model parameters of the SMO layers and we will consider anisotropy only in the LMO blocks with values of the ratio $t_z/t$ larger than unity and of the ratio $\epsilon_z/\epsilon$ smaller than unity.

Finally, to investigate the effects of the electron-lattice coupling, we will use the dimensionless quantity $\lambda$ defined as

$$\lambda = \frac{g^2 \omega_0}{6t}. \tag{4}$$

Throughout the paper, we will assume $\omega_0/t = 0.5$.

### B. Test Hamiltonian

In this work, we will consider solutions of the Hamiltonian that break the translational invariance in the out-of-plane $z$ direction. The thickness of the slab is a parameter of the system that will be indicated by $N_z$. We will build up a variational procedure including these features of the heterostructures. A simplified variational approach similar to that developed in this work has already been proposed by some of the authors for manganite bulks[23] and films.[24,25]

To treat variationally the electron-phonon interaction, the Hamiltonian (1) has been subjected to an inhomogeneous Lang-Firsov canonical transformation.[26] It is defined by parameters depending on plane indices along the $z$ direction:

$$U = \exp\left[ -g \sum_{i_{||}, i_z} \left( f_{i_z} c^\dagger_{i_{||}, i_z} c_{i_{||}, i_z} + \Delta_{i_z} \right) \left( a_{i_{||}, i_z} - a^\dagger_{i_{||}, i_z} \right) \right], \tag{5}$$

where $i_{||}$ indicates the in-plane lattice sites $(i_x, i_y)$, while $i_z$ are the sites along the direction $z$. The quantity $f_{i_z}$ represents the strength of the coupling between an electron and the phonon displacement on the same site belonging to the $i_z$ plane, hence it measures the degree of the polaronic effect. On the other hand, the parameter $\Delta_{i_z}$ denotes a displacement field describing static distortions that are not influenced by instantaneous position of the electrons.

To obtain an upper limit for free energy, the Bogoliubov inequality has been adopted:

$$F \leqslant F_{\text{test}} + \langle \tilde{H} - H_{\text{test}} \rangle_t, \tag{6}$$

where $F_{\text{test}}$ and $H_{\text{test}}$ are the free energy and the Hamiltonian corresponding to the test model that is assumed with an ansatz. $\tilde{H}$ stands for the transformed Hamiltonian $\tilde{H} = U H U^\dagger$. The symbol $\langle \rangle_t$ indicates a thermodynamic average performed by using the test Hamiltonian. The only part of $H_{\text{test}}$ that contributes to $\langle \tilde{H} - H_{\text{test}} \rangle_t$ is given by the spin degrees of freedom and depends on the magnetic order of the $t_{2g}$ core spins. For the spins, this procedure is equivalent to the standard mean-field approach.

The model test Hamiltonian, $H_{\text{test}}$, is such that that electron, phonon, and spin degrees of freedom are not interacting with each other:

$$H_{\text{test}} = H^{\text{sp}}_{\text{test}} + H^{\text{ph}}_{\text{test}} + H^{\text{el}}_{\text{test}}. \tag{7}$$

The phonon part of $H_{\text{test}}$ simply reads

$$H^{\text{ph}}_{\text{test}} = \omega_0 \sum_{i_{||}, i_z} a^\dagger_{i_{||}, i_z} a_{i_{||}, i_z}, \tag{8}$$

and the spin term is given by

$$H^{\text{sp}}_{\text{test}} = -g_S \mu_B \sum_{i_{||}} \sum_{i_z} h^z_{i_{||}, i_z} S^z_{i_{||}, i_z}, \tag{9}$$

where $g_S$ is the dimensionless electron-spin factor ($g_S \simeq 2$), $\mu_B$ is the Bohr magneton, and $h^z_{i_{||}, i_z}$ is the effective variational magnetic field. In this work, we consider the following magnetic orders modulated plane by plane:

$$\begin{aligned} F, &\quad h^z_{i_{||}, i_z} = \left| h^z_{i_z} \right|; \\ A, &\quad h^z_{i_{||}, i_z} = (-1)^{i_z} \left| h^z_{i_z} \right|; \\ C, &\quad h^z_{i_{||}, i_z} = (-1)^{ix+iy} \left| h^z_{i_z} \right|; \\ G, &\quad h^z_{i_{||}, i_z} = (-1)^{ix+iy+iz} \left| h^z_{i_z} \right|. \end{aligned} \tag{10}$$

For all these magnetic orders, the thermal averages of double-exchange operator, corresponding to neighboring sites in the same plane $i_z$ $\gamma_{i_z;i_{||},i_{||}+\delta_{||}}$ and in different planes $\eta_{i_z,i_z+\delta_z;i_{||}}$, preserve only the dependence on the $z$-plane index:

$$\gamma_{i_z;i_{||},i_{||}+\delta_{||}} = \left\langle \frac{S_0^{i_{||},i_z;i_{||}+\delta_{||},i_z} + 1/2}{2S+1} \right\rangle_t = \gamma_{i_z},$$
$$\eta_{i_z,i_z+\delta_z;i_{||}} = \left\langle \frac{S_0^{i_{||},i_z;i_{||},i_z+\delta_z} + 1/2}{2S+1} \right\rangle_t = \eta_{i_z,i_z+\delta_z}. \quad (11)$$

To get the mean-field electronic Hamiltonian, we make the Hartree approximation for the Coulomb interaction. The electronic contribution $H_{\text{test}}^{\text{el}}$ to the test Hamiltonian becomes

$$\begin{aligned} H_{\text{test}}^{\text{el}} = & -t \sum_{i_{||}} \sum_{i_z=1}^{N_z} \sum_{\delta_{||}} \gamma_{i_z} e^{-V_{i_z}} c^{\dagger}_{i_{||},i_z} c_{i_{||}+\delta_{||},i_z} \\ & - t_z \sum_{i_{||}} \sum_{i_z=1}^{N_z} \sum_{\delta_z} \eta_{i_z,i_z+\delta_z} e^{-W_{i_z,i_z+\delta_z}} c^{\dagger}_{i_{||},i_z} c_{i_{||},i_z+\delta_z} \\ & + \sum_{i_{||}} \sum_{i_z=1}^{N_z} [\phi_{\text{eff}}(i_z) - \mu]\, c^{\dagger}_{i_{||},i_z} c_{i_{||},i_z} \\ & + N_x N_y (T_1 + T_2) + N_x N_y g^2 \omega_0 \sum_{i_z} \Delta_{i_z}. \end{aligned} \quad (12)$$

In Eq. (12), the quantity $\phi_{\text{eff}}(i_z)$ indicates the effective potential seen by the electrons. It consists of the Hartree self-consistent potential $\phi(i_z)$ (see Appendix) and a potential due to the electron-phonon coupling:

$$\phi_{\text{eff}}(i_z) = \phi(i_z) + g^2 \omega_0 C_{i_z}, \quad (13)$$

with

$$C_{i_z} = f_{i_z}^2 - 2 f_{i_z} + 2\Delta_{i_z}(f_{i_z} - 1). \quad (14)$$

The factors $e^{-V_{i_z}}$ and $e^{-W_{i_z,i_z+\delta_z}}$ represent the phonon thermal average of Lang-Firsov operators:

$$e^{-V_{i_z}} = \left\langle X_{i_{||},i_z} X^{\dagger}_{i_{||}+\delta_{||},i_z} \right\rangle_t, \quad e^{-W_{i_z,i_z+\delta_z}} = \left\langle X_{i_{||},i_z} X^{\dagger}_{i_{||},i_z+\delta_z} \right\rangle_t, \quad (15)$$

where the operator $X_{\vec{R}_i}$ reads

$$X_{\vec{R}_i} = e^{g f_{i_z}(a_{\vec{R}_i} - a^{\dagger}_{\vec{R}_i})}.$$

Finally, the quantity $T_1$ and $T_2$ derive from the Hartree approximation (see Appendix), and $N_x$ and $N_y$ denote the size of the system along the two in-plane directions, respectively. To calculate the variational free energy, we need to know eigenvalues and eigenvectors of $H_{\text{test}}^{\text{el}}$ that depend on the magnetic order of core spins through the double-exchange terms.

### C. Magnetic order and diagonalization of the electronic mean-field Hamiltonian

To develop the calculation, we need to fix the magnetic order of core spins. The pattern of magnetic orders is determined by the minimization of the total free energy. By exploiting the translational invariance along the directions perpendicular to the growth axis of the heterostructure, the diagonalization for $H_{\text{test}}^{\text{el}}$ reduces to an effective unidimensional problem for each pair of continuous wave vectors $(k_x,k_y) = \vec{k}_{||}$. For some magnetic patterns, the electronic problem is characterized at the interface by a staggered structure. Therefore, we study the electron system considering a reduced first Brillouin zone of in-plane wave vectors. To this aim, we represent $H_{\text{test}}^{\text{el}}$ with the $2N_z$ states

$$|k_x,k_y,i_z\rangle, \quad |k_x+\pi,k_y+\pi,i_z\rangle, \quad (16)$$

with the wave vectors such that $-\pi/2 < k_x < \pi/2$, $-\pi/2 < k_y < \pi/2$, and $i_z$ going from 1 to $N_z$. The eigenstates of the electronic test Hamiltonian are indicated by $E(k_x,k_y,n)$, with the eigenvalue index $n$ going from 1 to $2N_z$. The eigenvector related to $n$ is specified in the following way: $b_{i_z}(\vec{k}_{||},n)$ for the first $N_z$ components, $p_{i_z}(\vec{k}_{||},n)$ for the remaining $N_z$ components.

The variational procedure is self-consistently performed by imposing that the total density of the system $\rho$ is given by $N_{\text{La}}/N_z$, with $N_{\text{La}}$ the number of layers of the LMO block, and the local plane density $\chi(i_z)$ is equal to $\langle n_{\vec{R}_i} \rangle$. Therefore, one has to solve the following $N_z + 1$ equations:

$$\rho = \frac{1}{N_x N_y N_z} \sum_{\vec{k}_{||}} \sum_{n} n_F[E(\vec{k}_{||},n)] \quad (17)$$

and

$$\begin{aligned} \chi(i_z) = \frac{1}{N_x N_y} \sum_{\vec{k}_{||}} \sum_{n} n_F[E(\vec{k}_{||},n)] \Big\{ & \left| b_{i_z}(\vec{k}_{||},n) \right|^2 + \left| p_{i_z}(\vec{k}_{||},n) \right|^2 \\ & + \left[ b^*_{i_z}(\vec{k}_{||},n) p_{i_z}(\vec{k}_{||},n) + p^*_{i_z}(\vec{k}_{||},n) b_{i_z}(\vec{k}_{||},n) \right] \Big\}, \end{aligned} \quad (18)$$

where $n_F(z)$ is the Fermi distribution function. These equations allow us to obtain the chemical potential $\mu$ and the local charge density $\chi(i_z)$. As a result of the variational analysis, one is able to get the charge-density profile corresponding to magnetic solutions that minimize the free energy.

## III. STATIC PROPERTIES AND PHASE DIAGRAMS

We have found the magnetic solutions and the corresponding density profiles that are stable for different sizes of the LMO and SMO blocks. The inhomogeneous variational approach allows us to determine the values of the electron-phonon parameters $f_{i_z}$ and $\Delta_{i_z}$ and the magnetic order of the $t_{2g}$ spins through the effective magnetic fields $h_{i_z}$. We will study the systems in the intermediate to strong electron-phonon regime characteristic of manganite materials focusing on two values of coupling: $\lambda = 0.5$ and 0.8. The maximum value of in-plane antiferromagnetic superexchange is $\epsilon = 0.01t$. The value of the Coulomb term $\alpha$ is fixed to $\alpha = 0.2$. We will analyze the heterostructures in the low-temperature regime: $T = 0.05t$.

The general structure of our solutions is characterized by three phases running along the $z$ direction. Actually, according to the parameters of the model, we find $G$ or $C$ antiferromagnetic phases corresponding to localized or delocalized charge carriers inside the LMO block, respectively. The localization is ascribed to the electron-phonon coupling, which gives rise to the formation of small polarons. For

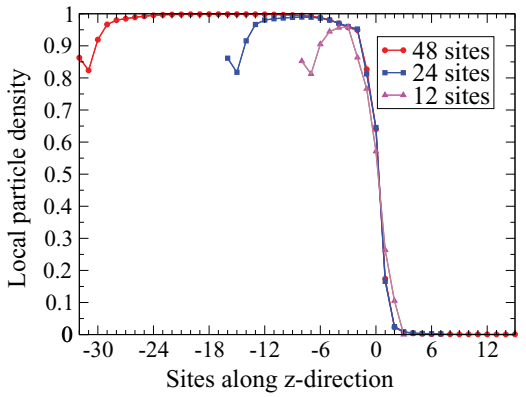


FIG. 1. (Color online) Comparison among density profiles corresponding to different sizes at $\lambda = 0.5$ and $\epsilon = 0.01t$. The index 0 indicates the interface Mn plane between the last La plane in the LMO block and the first Sr plane in the SMO block.

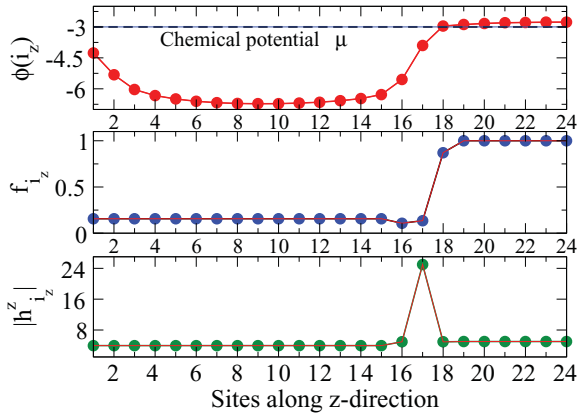


FIG. 2. (Color online) Self-consistent Hartree potential $\phi(i_z)$ (upper panel, in units of $t$), variational parameters $f_{i_z}$ (middle panel), and effective magnetic fields $|h^z_{i_z}|$ (lower panel) along the $z$ axis for $\lambda = 0.5$ and $\epsilon = 0.01t$.

the values of $\lambda$ considered in this paper, a ferromagnetic phase always stabilizes around the interface. The size of the ferromagnetic region at the interface is determined by the minimization of the free energy and depends on the values of the system parameters. Only for larger values of $\lambda$ and $\epsilon$ is the possibility of interface ferromagnetism forbidden. Inside the SMO block, a localized polaronic $G$-type antiferromagnet phase is always stable.

At first, we have analyzed the scaling of the static properties as a function of the size of the system along the $z$ growth direction. Therefore, a comparison of the density profiles has been done with $(LMO)_8/(SMO)_4$, $(LMO)_{16}/(SMO)_8$, and $(LMO)_{32}/(SMO)_{16}$ systems. In Fig. 1, we show the density profiles in a situation where strain-induced anisotropy has not been introduced. It is worth noticing that we indicate the interface Mn plane between the last La plane in the LMO block and the first Sr plane in the SMO block with the index 0. For a sufficiently large number of planes, the charge profile along $z$ shows a well-defined shape. Indeed, the local density is nearly unity in the LMO block, nearly zero in the SMO block, and it decreases from 1 to 0 in the interface region. The decrease of charge density for the first planes of LMO is due to the effect of open boundary conditions along the $z$ direction. In the intermediate electron-phonon coupling regime that we consider in Fig. 1, the region with charge dropping involves four to five planes between the two blocks. We notice that the local charge density for $(LMO)_{16}/(SMO)_8$ and $(LMO)_{32}/(SMO)_{16}$ systems is very similar around the interface. Furthermore, the numerical results show close values of variational free energy corresponding to the above-mentioned systems. Given the similarity of the properties of these two systems, in the following we will develop the analysis on the role of the interface studying the system $(LMO)_{16}/(SMO)_8$.

For the same set of electron-phonon and magnetic couplings, the variational parameters and the Hartree self-consistent potential along the $z$ axis are shown in Fig. 2. The effective magnetic fields are plotted for the most stable magnetic solution: antiferromagnetic $G$ orders well inside LMO (planes 1–15) and SMO (planes 19–24), and ferromagnetic planes at the interface (planes 16–18). The peak in the plot of the magnetic fields signals that ferromagnetism is quite robust at the interface. The variational electron-phonon parameters $f_{i_z}$ are small on the LMO side and at the interface, but close to unity in the SMO block. This means that, for these values of the couplings, carriers are delocalized in LMO up to the interface region, but small polarons are present in the SMO block. The quantities $\Delta_{i_z}$, which enter the variational treatment of the electron-phonon coupling, are determined by $f_{i_z}$ and the local density $\langle n_{i_z}\rangle$ through the equation $\Delta_{i_z} = \langle n_{i_z}\rangle(1 - f_{i_z})$. The Hartree self-consistent potential $\Phi$ indicates that charges are trapped into a potential well corresponding to the LMO block. Moreover, it is important to stress the energy scales involved in the well: the barrier between the LMO and SMO blocks is of the order of the electron bandwidth. Furthermore, at the interface, the energy difference between neighboring planes is of the order of the hopping energy $t$.

As mentioned above, for these systems, strain plays an important role. To study quantitatively its effect, we have investigated the phase diagram under the variation of the hopping anisotropy $t_z/t$ for two different values of $\epsilon_z$ ($\epsilon_z = \epsilon = 0.01t, \epsilon_z = 0$). Indeed, we simulate the compressive strain in the LMO block increasing the ratio $t_z/t$ and decreasing $\epsilon_z/\epsilon$. On the other hand, the tensile strain in the SMO block favors the more isotropic $x^2$-$y^2$ orbital and does not yield sizable effects. Therefore, for the SMO block, in the following we choose $t_z = t$ and $\epsilon_z = \epsilon$. For what concerns the electron-phonon interaction, we assume the intermediate coupling $\lambda = 0.8$. As shown in the upper panel of Fig. 3, upon increasing the ratio $t_z/t$ up to 1.7 for $\epsilon_z = \epsilon$, the magnetic order in LMO does not change since it remains $G$ antiferromagnetic. However, the character of charge carriers is varied. Actually, for $\lambda = 0.8$, in the absence of anisotropy, small polarons are present in the LMO block. Moreover, at $t_z/t \simeq 1.5$, in LMO, a change from small localized polarons to large delocalized polarons occurs. For all values of the ratio $t_z/t$, the interface region is characterized by ferromagnetic order with large polaron carriers and SMO by $G$ antiferromagnetic order with small polaron carriers.

It has been shown that it is also important to consider the anisotropy in superexchange ($\epsilon_z \neq \epsilon$) parameters as a consequence of strain.[22] To simulate the effect of compressive strain in LMO, a reduction of $\epsilon_z$ will be considered. We discuss the

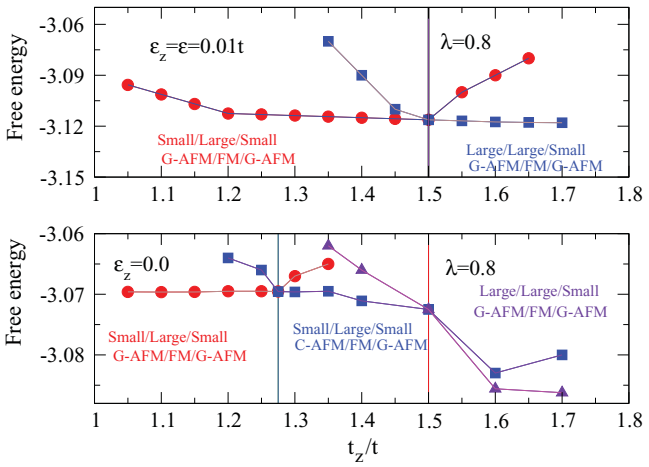


FIG. 3. (Color online) Phase diagram in the hopping anisotropy-energy plane for the $LMO_{16}SMO_8$ system, corresponding to $\lambda = 0.8$ for $\epsilon_z = 0.01t$ (upper panel) and $\epsilon_z = 0$ (lower panel).

limiting case $\epsilon_z = 0$. For this regime of parameters, the effect on the magnetic phases is the strongest. As shown in the lower panel of Fig. 3, for $1.28 \leqslant t_z/t \leqslant 1.5$, in the LMO block, a $C$-type antiferromagnetic phase is the most stable. The transition from small to large polarons again takes place at $t_z/t \simeq 1.5$. Therefore, we have shown that there is a range of parameters where the LMO block has $C$-type antiferromagnetic order with small localized polarons. Due to the effect of strain, the magnetic solution in LMO turns out to be compatible with experimental results in superlattices.[15] The interface is still ferromagnetic with metallic large polaron features. In the figure, $A/B/C$ refers to magnetic orders and the character of charge carriers inside LMO (A), at interface (B), inside SMO (C).

To analyze the effects of the electron-phonon interaction, a comparison between two different electron-phonon couplings is reported in Fig. 4. We have investigated the solutions that minimize the variational free energy at a fixed value of the anisotropy factors $t_z/t = 1.3$ and $\epsilon_z = 0$ at $\lambda = 0.5$ and 0.8. The magnetic solution in the LMO block is $C$ antiferromagnetic until the 15th plane. For both values of $\lambda$, polarons are small. In the SMO block, starting from the 19th plane, the solution is $G$-type antiferromagnetic together with localized polarons. Three planes around the interface are

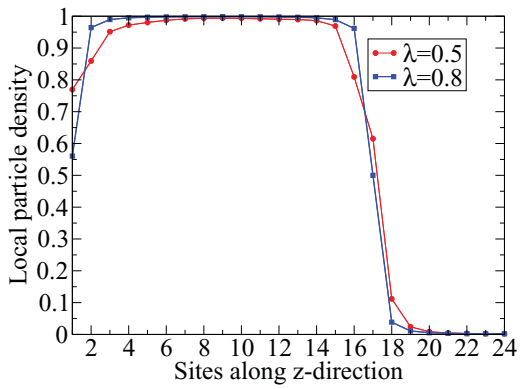


FIG. 4. (Color online) Comparison between local particle density corresponding to $\lambda = 0.5$ and 0.8 for $t_z/t = 1.3$ and $\epsilon_z = 0$.

TABLE I. Ratio between the magnetization and its saturation value for $\lambda = 0.5$ and 0.8 as a function of the anisotropy ratio $t_z/t$ for $\epsilon_z = 0$.

| $t_z/t$ | Magnetization ($\lambda = 0.5$) | Magnetization ($\lambda = 0.8$) |
|---|---|---|
| 1.0 | 0.1148 | 0.1090 |
| 1.1 | 0.1182 | 0.1123 |
| 1.2 | 0.1206 | 0.1146 |
| 1.3 | 0.1222 | 0.1161 |
| 1.4 | 0.1233 | 0.1172 |
| 1.5 | 0.1241 | 0.1179 |

ferromagnetically ordered. For $\lambda = 0.5$, all three planes at the interface are characterized by delocalized polarons, while for $\lambda = 0.8$, only the plane linking the ends of the LMO and SMO blocks is with delocalized charge carriers.

As shown in Fig. 4, the quantity $\lambda$ has important consequences on the physical properties, such as the local particle density. Actually, for $\lambda = 0.8$, the transition from occupied to empty planes is sharper at the interface. Only one plane at the interface shows an intermediate density close to 0.5. For $\lambda = 0.5$, the charge profile is smoother and the three ferromagnetic planes with large polarons have densities different from 0 and 1.

The last static quantity that we have evaluated is the magnetization. In Table I, we report the ratio between the magnetization of the heterostructure and the saturation value as a function of the anisotropy term $t_z/t$. We consider the case in which $\epsilon_z = 0$. Due to the formation of a few ferromagnetic planes at the interface, the magnetization ratio is very small (of the order of 0.1). Moreover, for $\lambda = 0.8$, its value is slightly smaller than 1 at $\lambda = 0.5$. The comparison with recent experimental data (see Ref. 9) on the single interface is very interesting. The order of magnitude of the calculated magnetization (about 0.12 times the saturation value per manganese at $t_z/t = 1.3$) is in good agreement with the experimental value at low temperature (0.162 times the saturation bulk ferromagnetic value per manganese). Therefore, not only the kind of magnetic order, but also the order of magnitude of magnetization compare quite well with experimental data.

For the analysis of the spectral and optical quantities, we will consider the parameters used for the discussion of the results in the last figure and the table focusing on $t_z/t = 1.3$.

## IV. SPECTRAL PROPERTIES

In this section, we will calculate the spectral properties of the heterostructure for the same parameters used in Fig. 4.

Performing the canonical transformation (5) and exploiting the cyclic properties of the trace, the electron Matsubara Green's function becomes

$$\mathcal{G}(\vec{R}_i, \vec{R}_j, \tau) = -\left\langle T_\tau c_{\vec{R}_i}(\tau) X_{\vec{R}_i}(\tau) c^\dagger_{\vec{R}_j}(0) X^\dagger_{\vec{R}_j}(0) \right\rangle. \quad (19)$$

By using the test Hamiltonian (7), the correlation function can be disentangled into electronic and phononic terms.[23,24] Going to Matsubara frequencies and making the analytic continuation $i\omega_n \to \omega + i\delta$, one obtains the retarded Green's function and

the diagonal spectral function $A_{i_z}^{i_x i_y}(\omega)$ corresponding to $\vec{R}_i = \vec{R}_j$,

$$A_{i_z}^{i_x,i_y}(\omega) = e^{S_T^{i_z}} \sum_{l=-\infty}^{\infty} I_l(S^{i_z}) e^{\frac{\beta l\omega_0}{2}} [1 - n_F(\omega - l\omega_0)] g_{i_z}^{i_x,i_y}(\omega - l\omega_0) + e^{S_T^{i_z}} \sum_{l=-\infty}^{\infty} I_l(S^{i_z}) e^{\frac{\beta l\omega_0}{2}} n_F(\omega + l\omega_0) g_{i_z}^{i_x,i_y}(\omega + l\omega_0), \quad (20)$$

where $S_T^{i_z} = g^2 f_{i_z}^2 (2N_0 + 1)$, $S^{i_z} = 2g^2 f_{i_z}^2 [N_0(N_0+1)]^{\frac{1}{2}}$, $I_l(z)$ are modified Bessel functions, and $g_{i_z}^{i_x,i_y}(\omega)$ is

$$g_{i_z}^{i_x,i_y}(\omega) = \frac{2\pi}{N_x N_y} \sum_{\vec{k}_{||}} \sum_{n=1}^{2N_z} \delta[\omega - E(\vec{k}_{||},n)] \{ |b_{i_z}(\vec{k}_{||},n)|^2 + |p_{i_z}(\vec{k}_{||},n)|^2 + (-1)^{i_x+i_y} [b_{i_z}^*(\vec{k}_{||},n) p_{i_z}(\vec{k}_{||},n) + p_{i_z}^*(\vec{k}_{||},n) b_{ic_z}(\vec{k}_{||},n)] \}. \quad (21)$$

The density of states $D(\omega)$ is defined as

$$D(\omega) = \frac{1}{N_x N_y N_z} \frac{1}{2\pi} \sum_{i_x,i_y,i_z} A_{i_z}^{i_x,i_y}(\omega). \quad (22)$$

In Fig. 5, we report the density of state of the system $(LMO)_{16}/(SMO)_8$. It has been calculated measuring the energy from the chemical potential $\mu$. This comparison has been made at fixed low temperature ($k_B T = 0.05t$), therefore we can consider the chemical potential very close to the Fermi energy of the system. At $\lambda = 0.5$, the spectral function exhibits a residual spectral weight at $\mu$. The main contribution to the density of states at the chemical potential $\mu$ comes from the three ferromagnetic large polaron planes at the interface. Indeed, the contributions due to the (LMO) and (SMO) blocks is negligible.

For stronger electron-phonon coupling at $\lambda = 0.8$, we observe an important depression of the spectral function at $\mu$. Hence the formation of a clear pseudogap takes place. This result is still compatible with the solution of our variational calculation since, for this value of $\lambda = 0.8$, there is only one plane with delocalized charge carriers that corresponds to the plane indicated as the interface ($i_z = 17$), while the two additional ferromagnetic planes around the interface are characterized by small polarons. The depression of the density of states at the Fermi energy is due also to the polaronic localization well inside the LMO and SMO block. In any case, we find that, even for $\lambda = 0.8$, the density of states never vanishes at the interface, in agreement with experimental results.[12]

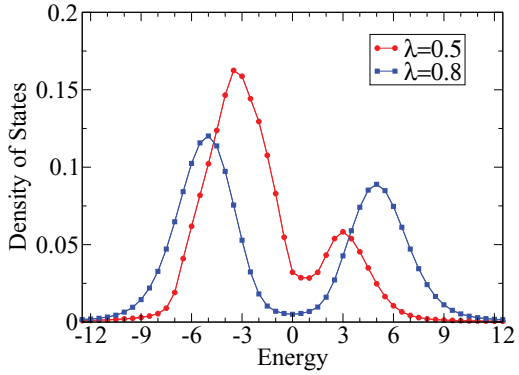


FIG. 5. (Color online) Comparison between density of states (in units of $1/t$) as a function of the energy (in units of $t$) corresponding to $\lambda = 0.5$ and 0.8.

In this section, we have found strong indications that a metallic ferromagnetic interface can form at the interface between LMO and SMO blocks. This situation should be relevant for superlattices with $n \geqslant 3$, where resistivity measurements made with contacts on top of LMO show a globally insulating behavior. In our analysis, we have completely neglected any effect due to disorder even if, both from experiments[8,9] and theories,[17] it has been suggested that localization induced by disorder could be the cause of the metal-insulator transition observed for $n \geqslant 3$. We point out that the sizable source of disorder due to the random doping with $Sr^{2+}$ is strongly reduced since, in superlattices, $La^{3+}$ and $Sr^{2+}$ ions are spatially separated by interfaces. Therefore, the amount of disorder present in the heterostructure is strongly reduced in comparison with the alloy. However, considering the behavior of the LMO (SMO) block as that of a bulk with a small amount of holes (particles), one expects that even a weak disorder induces localization. On the other hand, a weak disorder is not able to prevent the formation of the ferromagnetic metallic interface favored by the double-exchange mechanism and the charge transfer between the bulklike blocks: the states at the Fermi level due to the interface formation have enough density[12] so that they cannot be easily localized by weak disorder. In this section, we have shown that this can be the case in the intermediate electron-phonon coupling regime appropriate for LMO/SMO heterostructures.

In the next section, we will analyze the effects of electron-phonon coupling and strain on the optical conductivity in the same regime of the parameters considered in this section.

## V. OPTICAL PROPERTIES

To determine the linear response to an external field of frequency $\omega$, we derive the conductivity tensor $\sigma_{\alpha,\beta}$ by means of the Kubo formula. To calculate the absorption, we need only the real part of the conductivity,

$$\mathrm{Re}\sigma_{\alpha,\alpha}(\omega) = -\frac{\mathrm{Im}\Pi_{\alpha,\alpha}^{\mathrm{ret}}}{\omega}, \quad (23)$$

where $\Pi_{\alpha,\beta}^{\mathrm{ret}}$ is the retarded current-current correlation function. Following a well-defined scheme[23,24] and neglecting vertex corrections, one can get a compact expression for the real part of the conductivity $\sigma_{\alpha,\alpha}$. It is possible to get the conductivity both along the plane perpendicular to the growth axis, $\sigma_{xx}$, and parallel to it, $\sigma_{zz}$. To calculate the current-current correlation function, one can use the spectral function $A_{\vec{k}_{||};i_z,j_z}$ derived in the previous section exploiting the translational invariance

along the in-plane direction. It is possible to show that the components of the real part of the conductivity become

$$\mathrm{Re}[\sigma_{xx}](\omega) = \frac{e^2t^2}{N_xN_y}\sum_{k_x,k_y} 4sen^2(k_x)\frac{1}{N_z}\sum_{i_z,j_z}\gamma_{i_z}\gamma_{j_z} \times \frac{1}{\omega}\int_{-\infty}^{\infty}\frac{d\omega_1}{4\pi}[n_F(\omega_1-\omega)-n_F(\omega_1)] \times A_{k_x,k_y;i_z,j_z}(\omega_1-\omega)A_{k_x,k_y;i_z,j_z}(\omega_1) \quad (24)$$

and

$$\mathrm{Re}[\sigma_{zz}](\omega) = \frac{e^2t^2}{N_xN_y}\sum_{k_x,k_y}\frac{1}{N_z}\sum_{i_z,j_z}\sum_{\delta_{1z},\delta_{2z}}\delta_{1z}\delta_{2z}\eta_{i_z,i_z+\delta_{1z}}\eta_{j_z,j_z+\delta_{2z}}\frac{1}{\omega} \times \int_{-\infty}^{\infty}\frac{d\omega_1}{4\pi}[n_F(\omega_1-\omega)-n_F(\omega_1)] \times A_{k_x,k_y;i_z+\delta_{1z},j_z+\delta_{2z}}(\omega_1-\omega)A_{k_x,k_y;i_z,j_z}(\omega_1). \quad (25)$$

In Fig. 6, we report the in-plane conductivity as a function of the frequency at $\lambda = 0.5$ and 0.8. We have checked that the in-plane response mainly comes from the interface planes. Both conductivities are characterized by a Drude-like response at low frequency. Therefore, the in-plane conductivity provides a clear signature of the formation of the metallic ferromagnetic interface. However, due to the effect of the interactions, we have found that the low-frequency in-plane response is at least one order of magnitude smaller than that of free electrons in the heterostructures. Moreover, additional structures are present in the absorption with increasing energy. For $\lambda = 0.5$, a new band with a peak energy of the order of hopping $t = 2\omega_0$ is clear in the spectra. This structure can be surely ascribed to the presence of large polarons at the three interface planes.[23] Actually, this band comes from the incoherent multiphonon absorption of large polarons at the interface. This is also confirmed by the fact that this band is quite broad, therefore it can be interpreted in terms of multiple excitations. For $\lambda = 0.8$, the band is even larger and shifted at higher energies. In this case, at the interface, large and small polarons are present with a ferromagnetic spin order. Therefore, there is a mixing of excitations whose net effect is the transfer of spectral weight at higher frequencies.

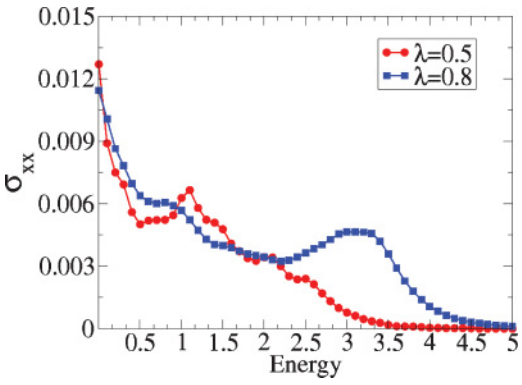


FIG. 6. (Color online) The conductivity [in units of $e^2/(mt)$, with $m = 1/(2t)$] into the plane perpendicular to the growth direction of the $(LMO)_{16}/(SMO)_8$ bilayer as a function of the energy (in units of $t$) for different values of $\lambda$.

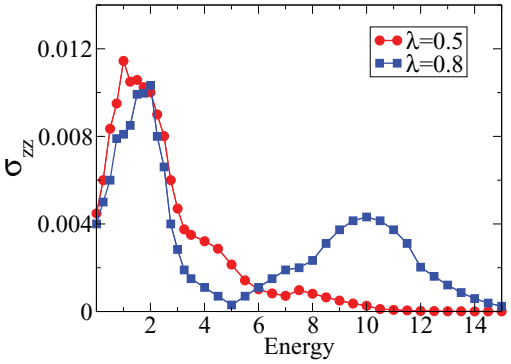


FIG. 7. (Color online) The conductivity [in units of $e^2/(mt)$, with $m = 1/(2t)$] along the growth direction of the $(LMO)_{16}(SMO)_8$ bilayer as a function of the energy (in units of $t$) for $\lambda = 0.5$ and 0.8.

The out-of-plane optical conductivities show significant differences in comparison with the in-plane responses. In Fig. 7, we report out-of-plane conductivity as a function of the frequency at $\lambda = 0.5$ and 0.8. First, we observe the absence of the Drude term. Moreover, the band at energy about $2\omega_0$ is narrower than that in the in-plane response. Therefore, the origin of this band has to be different. Actually, the out-of-plane optical conductivities are sensitive to the interface region. A charge carrier at the interface has to overcome an energy barrier to hop to the neighbor empty site. As shown in Fig. 2, the typical energy for close planes at the interface is of the order of the hopping $t$. Therefore, when one electron hops along $z$, it has to pay at least an energy of the order of $t$. In the out-of-plane spectra, the peaks at low energy can be ascribed to this process. Of course, by paying a larger energy, the electron can hop to the next nearest neighbors. This explains the width of this band due to interplane hopping.

Additional structures are present at higher energies in the out-of-plane conductivities. For $\lambda = 0.5$, the band at high energy is broad with small spectral weight. For $\lambda = 0.8$, there is an actual transfer of spectral weight at higher energies. A clear band is peaked around $10t$. This energy scale can be interpreted as given by $2g^2\omega_0 = 9.6t$ for $\lambda = 0.8$. Therefore, in the out-of-plane response, the contribution at high energy can be interpreted as due to small polarons.[23,27]

Unfortunately, experimental data about optical properties of the LMO/SMO bilayers are still not available. Therefore, comparison with experiments is not possible. Predictions on the different behaviors among $\sigma_{xx}$ and $\sigma_{zz}$ can be easily checked if one uses in-plane and out-of-plane polarization of the electrical fields used in the experimental probes. More importantly, the formation of two-dimensional gas at the interface is expected to be confirmed by experiments made by using lateral contacts directly on the region between the LMO and SMO blocks. The dc conductivity of the sheet could directly measure the density of carriers of the interface metal and confirm the Drude-like low-frequency behavior of in-plane response.

Finally, we have evaluated the conductivity of the entire system at zero frequency for different values of model parameters. In Fig. 8 , we report the in-plane (upper panel) and out-of-plane (lower panel) conductivity as a function of the anisotropy ratio $t_z/t$ for $\lambda = 0.5$ and 0.8. As expected, the

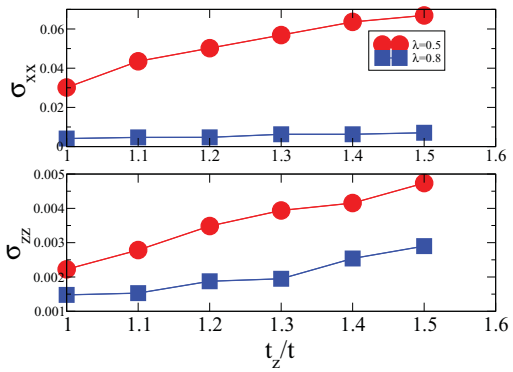


FIG. 8. (Color online) The conductivity at zero frequency [in units of $e^2/(mt)$, with $m = 1/(2t)$] of the $(LMO)_{16}(SMO)_8$ bilayer into the plane perpendicular to the growth direction (upper panel) and along the growth direction (lower panel) as a function of the anisotropy ratio $t_z/t$ for $\lambda = 0.5$ and 0.8.

conductivity gets larger upon increasing the ratio $t_z/t$ since ferromagnetic solutions are favored. Moreover, we point out that the out-of-plane conductivity is one order of magnitude less than the in-plane conductivity. The order of magnitude of the resistivity has been estimated considering the out-of-plane contribution of the calculated conductivity. For $t_z/t = 1.3$, the resistivity is about 0.2 Ω cm, a value that is comparable with experimental results at low temperature for the single interface (of the order of 1 Ω cm).[9] It is clear that disorder effects present in the material (not included in our analysis) should increase the value of resistivity by enhancing the scattering rate of the carriers. Therefore, a value of resistivity smaller than the experimental value is compatible with the complexity of these heterostructures.

## VI. CONCLUSIONS

In this paper, we have discussed phase diagrams and spectral and optical properties for a very large bilayer $(LMO)_{2n}/(SMO)_n$ (up to 48 sites along the growth direction). A correlated inhomogeneous mean-field approach has been developed to analyze the effects of electron-lattice antiadiabatic fluctuations and strain. We have shown that a metallic ferromagnetic interface is a quite robust feature of these systems for a large range of the electron-lattice couplings and strain strengths. Furthermore, we have found that the size of the interface region depends on the strength of electron-phonon interactions. At low temperature, the general structure of our solutions is characterized by three phases running along the growth $z$ direction: antiferromagnetic phase with localized and/or delocalized charge carriers inside the LMO block, ferromagnetic state with itinerant carriers at the interface, and localized polaronic $G$-type antiferromagnetic phase inside the SMO block. The type of antiferromagnetic order inside LMO depends on the strain induced by the substrate.

Spectral and optical properties have been discussed for different parameter regimes. Due to the formation of the metallic interface, even in the intermediate to strong electron-phonon coupling regime, the density of states never vanishes at the chemical potential. Finally, in-plane and out-of-plane optical conductivities are sharply different: the former shows a metallic behavior, the latter a transfer of spectral weight at high frequency due to the effects of the electrostatic potential well trapping electrons in the LMO block. The in-plane response provides a signature of the formation of the metallic ferromagnetic interface.

The approach proposed in this paper is accurate for the calculation of static properties. With regard to dynamical quantities, the role of the electron-phonon coupling is properly taken into account, while the effect of Coulomb interactions is considered only within mean field. To this aim, it could be interesting to improve the treatment of electron-electron interactions, for example, by using the random-phase approximation.[27] It is clear that the random-phase treatment is quite complex in heterostructures due to the lack of translational invariance along one direction. Moreover, the dynamical screening is poor due to the presence of large insulating antiferromagnetic blocks in the system. For this reason, the self-consistent mean-field approach is reasonable, simple, and able to grasp the main features of the effects of the Coulomb interactions.

In this paper, we have emphasized the role of polaron quasiparticles since they represent one of the main ingredients for the interpretation of the data in manganites.[4] Within our approach, the main contribution to the polaron formation comes from the local interaction. Other effects, such as those relative to cooperative interactions between vibrational modes, could make a contribution to the polaron formation. Moreover, coupling between Jahn-Teller modes on different sites could also improve the analysis of strain effects in the system. However, it is important to point out that our treatment of electron-phonon interaction is based on an inhomogeneous approach. Therefore, through kinetic-energy terms, correlations between different sites are assured.

Finally, we have focused on static and dynamic properties at very low temperature. The approach used in the paper is valid at any temperature. Therefore, it could be very interesting to analyze not only single interfaces but also superlattices with different unit cells at finite temperature. Work in this direction is in progress.

## APPENDIX

In this Appendix, we give some details about the effective electronic Hamiltonian derived within our approach. After the Hartree approximation for the long-range Coulomb interactions, the mean-field electronic Hamiltonian reads

$$
\begin{aligned}
H^{\mathrm{el}}_{\mathrm{test}} = & -t \sum_{i_\parallel} \sum_{i_z=1}^{N_z} \sum_{\delta_\parallel} \gamma_{i_z} e^{-V_{i_z}} c^\dagger_{i_\parallel,i_z} c_{i_\parallel+\delta_\parallel,i_z} \\
& - t \sum_{i_\parallel} \sum_{i_z=1}^{N_z} \sum_{\delta_z} \eta_{i_z,i_z+\delta_z} e^{-W_{i_z,i_z+\delta_z}} c^\dagger_{i_\parallel,i_z} c_{i_\parallel,i_z+\delta_z} \\
& + \sum_{i_\parallel} \sum_{i_z=1}^{N_z} [\phi(i_z) - \mu] c^\dagger_{i_\parallel,i_z} c_{i_\parallel,i_z} + N_x N_y (T_1 + T_2) \\
& + N_x N_y g^2 \omega_0 \sum_{i_z} \Delta_{i_z} + \sum_{i_\parallel} \sum_{i_z=1}^{N_z} C_{i_z} (g^2\omega_0) c^\dagger_{i_\parallel,i_z} c_{i_\parallel,i_z}.
\end{aligned}
\tag{A1}
$$

The self-consistent Hartree potential is given by

$$\phi(i_z) = \frac{e^2}{\epsilon}\left( \sum_{j_z>i_z} \chi(j_z)S(i_z - j_z) + \sum_{j_z<i_z} \chi(j_z)S(i_z - j_z) + S_1(0)\chi(i_z) - S_2(i_z)\right), \quad \text{(A2)}$$

where the quantity $T_1$ is

$$T_1 = \frac{-e^2}{2\epsilon}\left( \sum_{i_z=1}^{N_z}\sum_{j_z>i_z}^{N_z} \chi_{i_z}\chi_{j_z}S(i_z - j_z) + \sum_{j_z<i_z}^{N_z} \chi_{i_z}\chi_{j_z}S(i_z - j_z) + S_1(0)\sum_{i_z}^{N_z}\chi_{i_z}^2\right), \quad \text{(A3)}$$

and $T_2$ is

$$T_2 = \frac{e^2}{2\epsilon}\left( \sum_{I_z=1}^{N_{\rm La}}\sum_{J_z>I_z}^{N_{\rm La}} S(I_z - J_z) + \sum_{J_z<I_z}^{N_{\rm La}} S(I_z - J_z) + N_{\rm La}S_1\right), \quad \text{(A4)}$$

with $S(n_z)$, $S_1(0)$, and $S_2(n_z)$ obtained by adding the Coulomb terms on the in-plane lattice index. The summations have been made modulating the Coulomb interaction with a screening factor: $\frac{e^2}{|\vec{r}_i - \vec{r}_j|} \to \frac{e^2 e^{-\eta_S|\vec{r}_i - \vec{r}_j|}}{|\vec{r}_i - \vec{r}_j|}$, where $\frac{1}{\eta_S}$ is a fictitious finite screening length in units of the lattice parameter $a$. Therefore, $S(n_z)$ is

$$S(n_z) = \sum_{m_x,m_y} \frac{\exp\left(-\eta_S\sqrt{m_x^2 + m_y^2 + n_z^2}\right)}{\sqrt{m_x^2 + m_y^2 + n_z^2}}, \quad \text{(A5)}$$

$S_1(0)$ is given by

$$S_1(0) = \sum_{m_x,m_y} \frac{\exp\left(-\eta_S\sqrt{m_x^2 + m_y^2}\right)}{\sqrt{m_x^2 + m_y^2}}, \quad \text{(A6)}$$

with $(m_x,m_y) \neq (0,0)$, and $S_2(i_z - j_z)$ is

$$S_2(n_z) = \sum_{m_x,m_y}\sum_{i_z=1}^{l_z} \frac{\exp\left(-\eta_S\sqrt{h_x^2 + h_y^2 + h_z^2}\right)}{\sqrt{h_x^2 + h_y^2 + h_z^2}}, \quad \text{(A7)}$$

with $l_z$ the number of planes of the LMO block, $h_x = m_x - 0.5$, $h_y = m_y - 0.5$, and $h_z = n_z - i_z - 0.5$.


[1] M. Imada, A. Fujimori, and Y. Tokura, Rev. Mod. Phys. **70**, 1039 (1998).

[2] E. Dagotto, *Nanoscale Phase Separation and Colossal Magnetoresistance* (Springer-Verlag, Heidelberg, 2003).

[3] C. Zener, Phys. Rev. **81**, 440 (1951); **82**, 403 (1951); P. W. Anderson and H. Hasegawa, *ibid.* **100**, 675 (1955); P. G. de Gennes, *ibid.* **118**, 141 (1960).

[4] A. J. Millis, Nature (London) **392**, 147 (1998).

[5] A. Ohtomo and H. Y. Hwang, Nature (London) **419**, 378 (2002); S. Okamoto and A. J. Millis, *ibid.* **428**, 630 (2004).

[6] A. Ohtomo and H. Y. Hwang, Nature (London) **427**, 423 (2004); S. Thiel, G. Hammerl, A. Schmehl, C. W. Schneider, and J. Mannhart, Science **313**, 1942 (2006); N. Reyren, *ibid.* **317**, 1196 (2007).

[7] T. Koida, M. Lippmaa, T. Fukumura, K. Itaka, Y. Matsumoto, M. Kawasaki, and H. Koinuma, Phys. Rev. B **66**, 144418 (2002); H. Yamada, M. Kawasaki, T. Lottermoser, T. Arima, and Y. Tokura, Appl. Phys. Lett. **89**, 052506 (2006).

[8] A. Bhattacharya, S. J. May, S. G. E. te Velthuis, M. Warusawithana, X. Zhai, B. Jiang, J. M. Zuo, M. R. Fitzsimmons, S. D. Bader, and J. N. Eckstein, Phys. Rev. Lett. **100**, 257203 (2008).

[9] C. Adamo, X. Ke, P. Schiffer, A. Soukiassian, M. Warusawithana, L. Maritato, and D. G. Schlom, Appl. Phys. Lett. **92**, 112508 (2008).

[10] C. Adamo, C. A. Perroni, V. Cataudella, G. De Filippis, P. Orgiani, and L. Maritato, Phys. Rev. B **79**, 045125 (2009).

[11] N. Ogawa, T. Satoh, Y. Ogimoto, and K. Miyano, Phys. Rev. B **78**, 212409 (2008).

[12] S. Smadici, P. Abbamonte, A. Bhattacharya, X. Zhai, B. Jiang, A. Rusydi, J. N. Eckstein, S. D. Bader, and J.-M. Zuo, Phys. Rev. Lett. **99**, 196404 (2007).

[13] N. Ogawa, T. Satoh, Y. Ogimoto, and K. Miyano, Phys. Rev. B **80**, 241104(R) (2009).

[14] B. R. K. Nanda and S. Satpathy, Phys. Rev. Lett. **101**, 127201 (2008); Phys. Rev. B **79**, 054428 (2009).

[15] C. Aruta, C. Adamo, A. Galdi, P. Orgiani, V. Bisogni, N. B. Brookes, J. C. Cezar, P. Thakur, C. A. Perroni, G. De Filippis, V. Cataudella, D. G. Schlom, L. Maritato, and G. Ghiringhelli, Phys. Rev. B **80**, 140405(R) (2009).

[16] H. Yamada, P. H. Xiang, and A. Sawa, Phys. Rev. B **81**, 014410 (2010).

[17] S. Dong, R. Yu, S. Yunoki, G. Alvarez, J.-M. Liu, and E. Dagotto, Phys. Rev. B **78**, 201102(R) (2008); R. Yu, S. Yunoki, S. Dong, and E. Dagotto, *ibid.* **80**, 125115 (2009).

[18] C. Lin and A. J. Millis, Phys. Rev. B **78**, 184405 (2008).

[19] B. R. K. Nanda and S. Satpathy, Phys. Rev. B **78**, 054427 (2008); **81**, 224408 (2010).

[20] C. Lin, S. Okamoto, and A. J. Millis, Phys. Rev. B **73**, 041104(R) (2006).

[21] S. Dong, S. Yunoki, X. Zhang, C. Sen, J.-M. Liu, and E. Dagotto, Phys. Rev. B **82**, 035118 (2010).

[22] Z. Fang, I. V. Solovyev, and K. Terakura, Phys. Rev. Lett. **84**, 3169 (2000).

[23] C. A. Perroni, G. De Filippis, V. Cataudella, and G. Iadonisi, Phys. Rev. B **64**, 144302 (2001).

[24] C. A. Perroni, V. Cataudella, G. De Filippis, G. Iadonisi, V. Marigliano Ramaglia, and F. Ventriglia, Phys. Rev. B **68**, 224424 (2003).

[25] A. Iorio, C. A. Perroni, G. De Filippis, V. Marigliano Ramaglia, and V. Cataudella, J. Phys. Condens. Matter **21**, 456002 (2009).

[26] I. J. Lang and Yu. A. Firsov, Sov. Phys. JETP **16**, 1301 (1963).

[27] G. Mahan, *Many-Particle Physics*, 2nd ed. (Plenum, New York, 1990).